Supplementary Information.

a

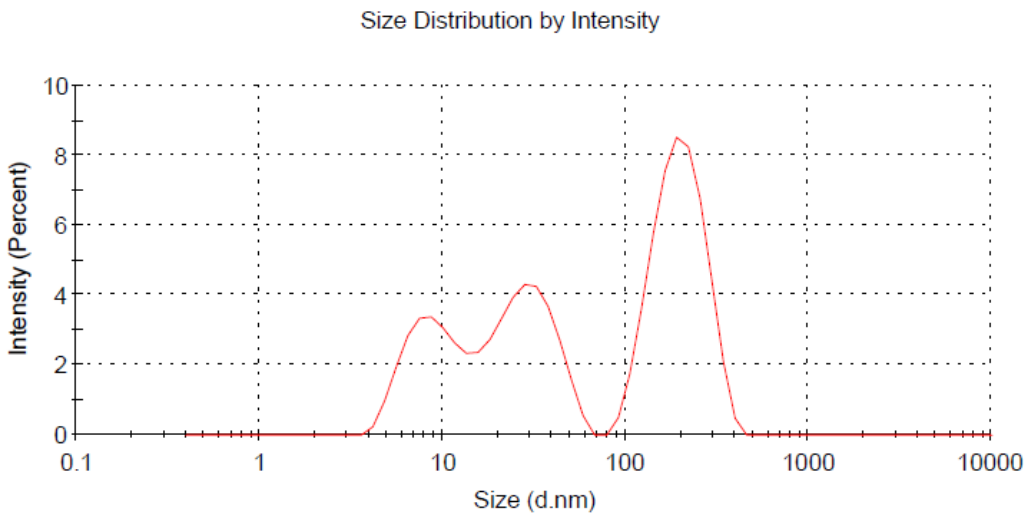

Results

			Size (d.n...	% Intensity:	St Dev (d.n...
Z-Average (d.nm):	98.96	**Peak 1:**	203.4	48.6	63.22
PdI:	0.265	**Peak 2:**	28.81	31.0	10.90
Intercept:	0.914	**Peak 3:**	8.819	20.3	2.603

b

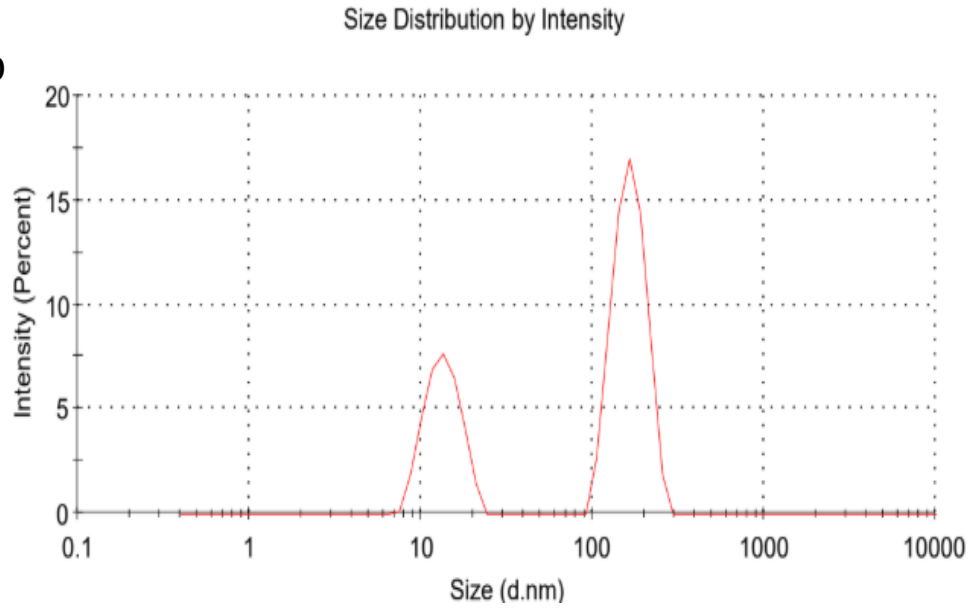

Results

			Size (d.n...	% Intensity:	St Dev (d.n...
Z-Average (d.nm):	507.0	**Peak 1:**	166.6	66.8	34.88
PdI:	0.540	**Peak 2:**	13.69	33.2	3.125
Intercept:	0.404	**Peak 3:**	0.000	0.0	0.000

Supplementary Figure S1. Dynamic light scattering (DLS) intensity-weighted size distributions of salivary extracellular vesicles. (a) Representative DLS profile showing a multimodal size distribution with peaks at ~8.8 nm, ~28.8 nm, and ~203.4 nm, with a Z-average diameter of ~99 nm and a polydispersity index (PDI) of 0.265, indicating moderate heterogeneity. (b) Representative DLS profile from a distinct sample exhibiting a dominant population at ~166.6 nm and a secondary peak at ~13.7 nm, with a Z-average diameter of ~507 nm and higher polydispersity (PDI = 0.540), reflecting the presence of larger particles or aggregates. Intensity-weighted distributions emphasize larger vesicles due to scattering bias.

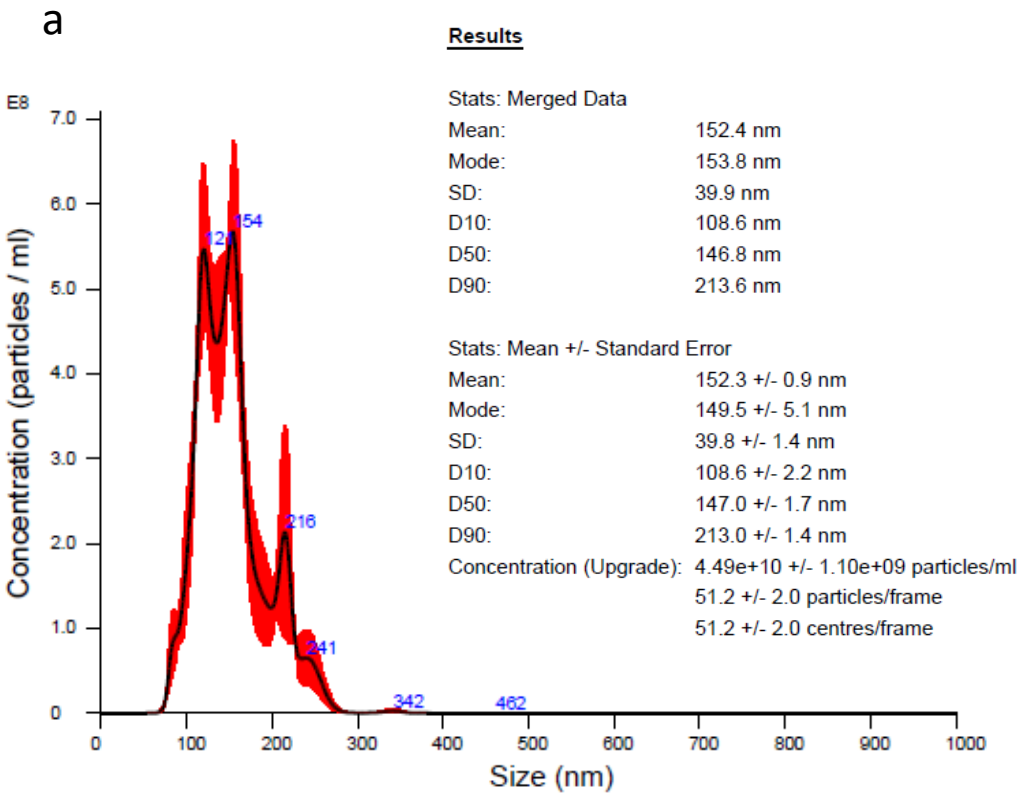

b

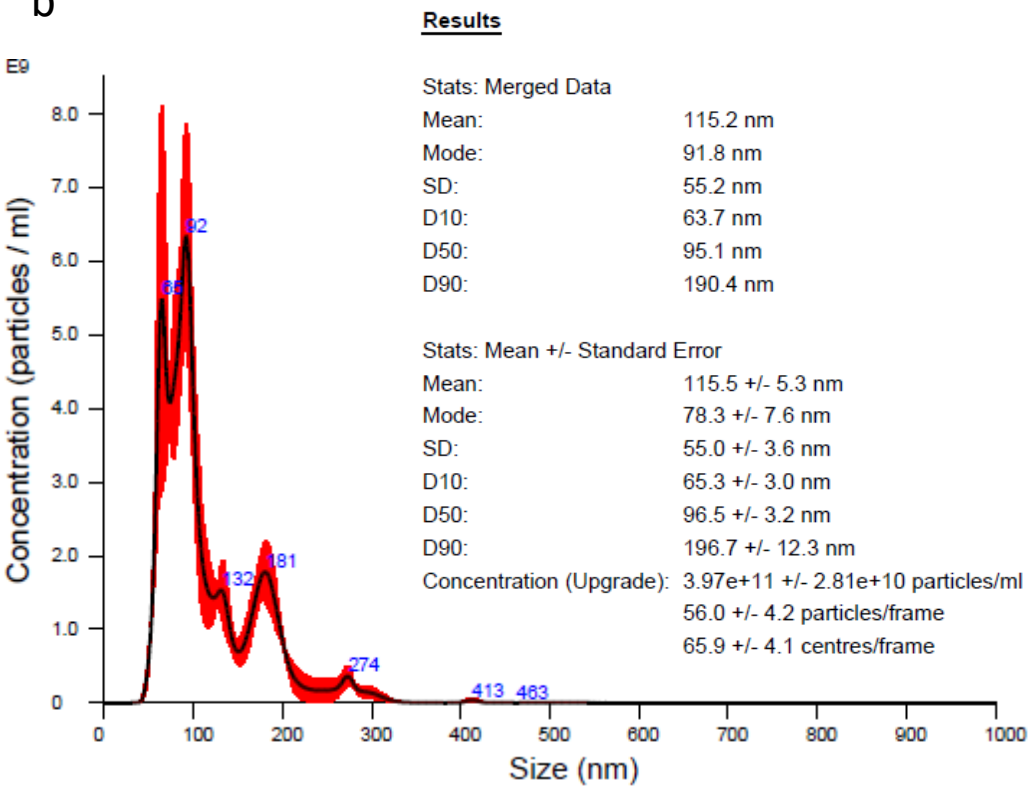

Supplementary Figure S2. Nanoparticle tracking analysis (NTA) size distribution profiles of salivary extracellular vesicles. (a) Representative NTA size distribution showing a predominant EV population centered at ~150 nm (mean ~152.4 nm; mode ~153.8 nm), with particle concentration of ~4.49 × 10^{10} particles/mL and a distribution spanning ~100–250 nm. (b) Representative NTA profile from a distinct sample demonstrating a dominant population at smaller diameters (mean ~115.2 nm; mode ~91.8 nm), with particle concentration of ~3.97 × 10^{11} particles/mL. Distribution percentiles (D10, D50, D90) confirm that the majority of particles fall within the expected size range for small extracellular vesicles. These results highlight inter-sample variability while maintaining a consistent nanoscale EV population characteristic of exosome-enriched fractions.

a

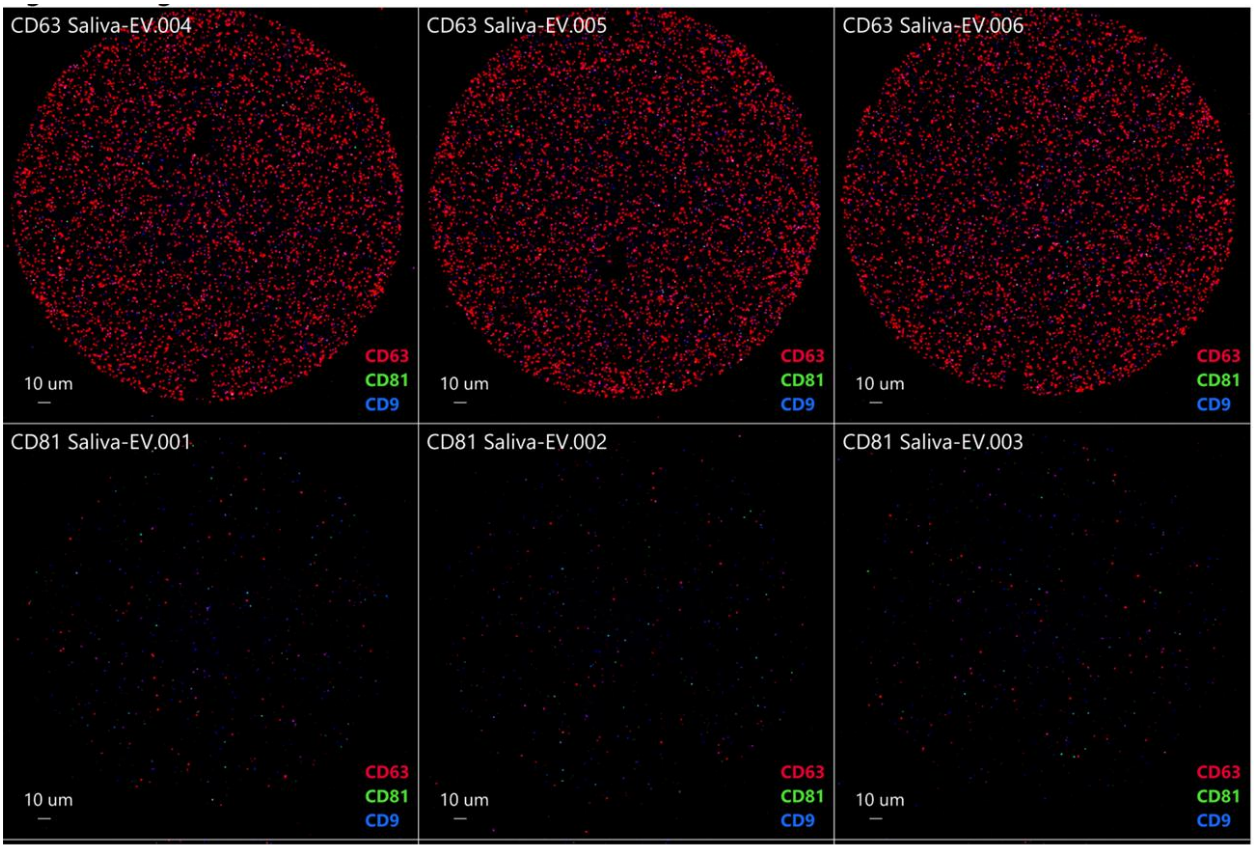
CD63 Saliva-EV.004
CD63 Saliva-EV.005
CD63 Saliva-EV.006
CD81 Saliva-EV.001
CD81 Saliva-EV.002
CD81 Saliva-EV.003
CD63
CD81
CD9
10 um

b

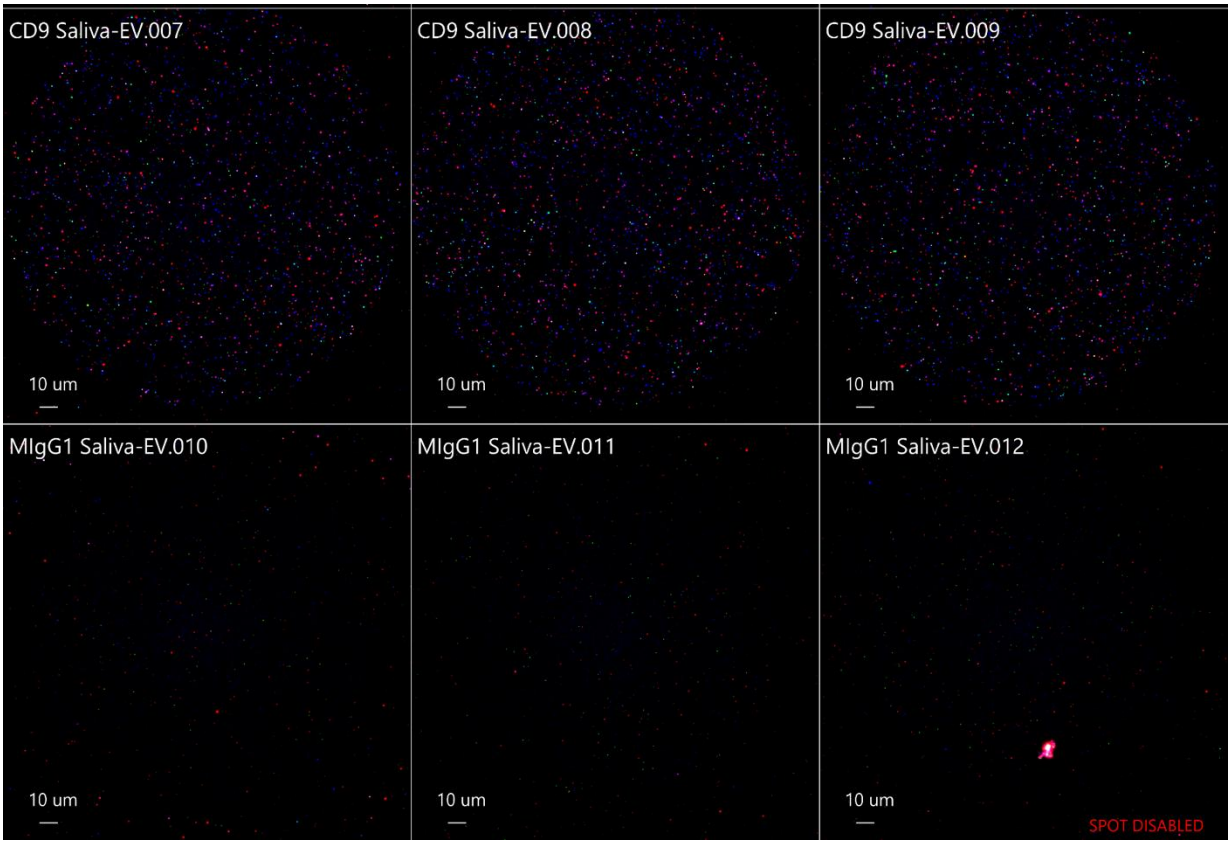
CD9 Saliva-EV.007
CD9 Saliva-EV.008
CD9 Saliva-EV.009
MIgG1 Saliva-EV.010
MIgG1 Saliva-EV.011
MIgG1 Saliva-EV.012
10 um
SPOT DISABLED

Supplementary Figure S3. Representative ExoView interferometric and fluorescence images of salivary extracellular vesicles across capture antibodies and controls. (a) Representative ExoView images of EVs captured using anti-CD63 and anti-CD81 antibodies from independent samples (n = 3 per condition). CD63 capture surfaces show dense particle binding with predominant CD63 signal (red), whereas CD81 capture surfaces exhibit lower particle density with detectable CD81 (green) and co-localized signals, reflecting variability in marker expression across EV subpopulations. (b) Representative images of EVs captured using anti-CD9 antibodies and IgG1 isotype control. CD9 capture surfaces display moderate particle binding with mixed fluorescence signals (blue), while IgG1 controls show minimal non-specific binding, confirming assay specificity. Fluorescence channels correspond to CD63 (red), CD81 (green), and CD9 (blue). Scale bars, 10 μm.

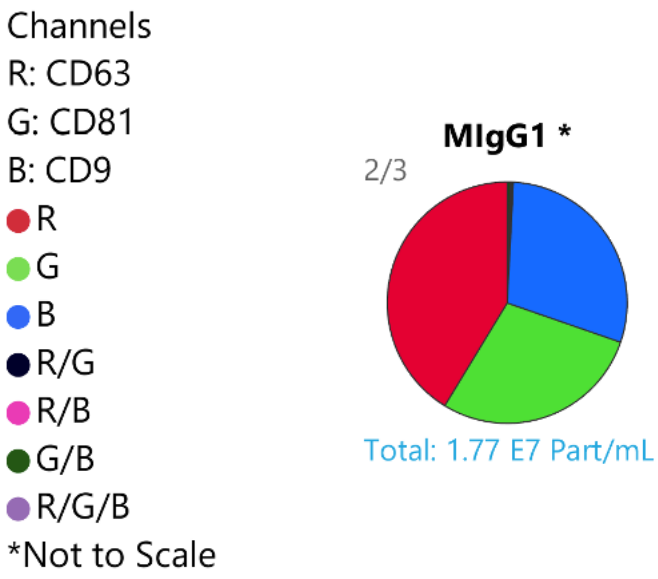

Supplementary Figure S4. Isotype control analysis of non-specific binding in ExoView measurements. Representative colocalization profile obtained from IgG1 isotype control capture surfaces, demonstrating minimal non-specific binding across fluorescence channels. Pie chart representation shows the distribution of detected signals corresponding to CD63 (red), CD81 (green), and CD9 (blue), with negligible co-localization events. The low particle count (total ~1.77 × 10^7 particles/mL) and absence of structured marker-specific patterns confirm the specificity of antibody-based EV capture in experimental conditions. Fluorescence channel assignments are indicated, and proportions are not to scale.